Metrol. Meas. Syst., Vol. 27 (2020) No. 2, pp. 243–263
DOI: 10.24425/mms.2020.132772

METROLOGY AND MEASUREMENT SYSTEMS
Index 330930, ISSN 0860-8229
www.metrology.wat.edu.pl

COMPARISONS OF ENVELOPE MORPHOLOGICAL FILTERING METHODS AND VARIOUS REGULAR ALGORITHMS FOR SURFACE TEXTURE ANALYSIS

Przemysław Podulka

Rzeszów University of Technology, Faculty of Mechanical Engineering and Aeronautics, al. Powstańców Warszawy 12, 35-959 Rzeszów, Poland (✉ *p.podulka@prz.edu.pl*, +48 17 743 2537)

Abstract

In this paper both envelope approach and morphological filters for characterisation of surface textures were proposed, applied and thoroughly examined. Obtained results were compared with those received after appliance of commonly-used algorithms. The effect of appliance of proposed procedures on surface topography parameters (from ISO 25178 standard) was taken into consideration. The following types of surface textures were assessed: two-process plateau-honed cylinder liners, plateau-honed cylinder liners with additionally burnished dimples, turned piston skirts, grinded and/or isotropic topographies. It was assumed that envelope characteristics (envelope filtration) can provide results useful for assessments of deep and/or wide oil-reservoirs especially when they are edge located. Moreover, some near-valley areas of surface texture details can be less distorted when envelope filtering is accomplished. It was also found that closing and/or opening envelope filtration can be valuable for reduction of some surface topography measurement errors.

Keywords: surface texture, surface topography measurement, envelope filter, morphological filtering, measurement errors.

1. Introduction

Importance of a comprehensive analysis of surface texture, considering both measurement and/or data processing etc., is revealed by thorough evaluation of mechanical behavior of engineering-determined surfaces. Furthermore, detailed assessment of surface topographies is recognized as an integral part of process control. There are many measurement systems integrated into the manufacturing process to provide a real-time feedback, some using analysis of features generated by a robotized surface finishing systems. Extraction and subsequent assessments of selected surface topography features can be perceived as being of remarkable value when tribological behavior of machined parts is taken into consideration in more detail. Moreover, feature-based characterization of surface textures was performed for many tribological performances [1, 2].

Evaluation of surface functional properties (*e.g.* lubricant retention, wear resistance) is closely dependent on the precision of surface texture measurement and analysis. Therefore both measurement accuracy and data processing methods should be considered as an absolutely essential in surface topography assessments. Errors in surface texture properties estimation can be divided basically into errors caused by the environment [3], measuring equipment, measured object [4], software and/or measuring method. Additionally, the errors obtained when the received measuring data is processed can be classified into errors in establishing the reference plane (extraction of functional features) and errors of computing parameters. In practice, both types of errors are closely related when data processing occurs.

A typical example of surface textures defined as stratified are the surface topographies of engine's piston-piston rings-cylinder liner system details. An analysis of the piston group components from car engines, *e.g.* cylinder liners, rings and pistons, is of an immense importance since up to 50% of the total energy is lost due to friction of these elements [5]. Besides, reducing fuel consumption and CO_2 emissions has a beneficial importance in environmental protection as well. Therefore, elements of this system should be subjected to strict control in the process of surface metrology [6].

Currently, optical methods are highly popular in surface metrology ; substantial advance has been made in the development of this type of surface topography measurements [7, 8]. Stylus methods are robust but slow [9] while the optical approaches are fast but particularly susceptible to extraneous effects. When the texture contains sharp edges, inclusions, defects or simply "peculiarities" – outliers or other dropouts (*e.g.* spikes [10], also called "sharp spikes" [11]) of measured data points can be predominantly found. Problem of unmeasured points in surface metrology was also carefully considered in [12]. Among optical methods *Scanning White-Light Interference* (SWLI) Microscopy is often called a "mature technology" or "probably the most useful optical instrument" [13] for measuring surfaces, films or coatings. Nevertheless, plenty of external factors can cause a noise with a different bandwidth [14]. There are various types of noise which can be roughly divided into: scattering noise [15], background noise [16], static noise [17], measurement noise [18] or other noise-like errors [19].

Extraction of some texture features by morphological filtering methods [20, 21] was often proposed and correlated with various commonly-used procedures, *e.g.* motif [22]. Analyses were performed for both 3D (surface) [23] and 2D (profile) [24–26] assessments. Three-dimensional filtering of engineering surfaces was also directly applied with envelope characterization [27, 28] or morphological closing filters [29].

In this paper envelope filter was proposed for extraction of some features from cylinder liner surface textures containing deep/wide oil pockets. Results were compared with those obtained after application of ordinarily proposed approaches, *e.g.* regular Gaussian regression filter [30] and those with robust modifications [31, 32], polynomials (from 2^{nd} to 4^{th} degree) or available in measuring instrument software spline filter [33]. Furthermore, it was also suggested to apply an opening-closing morphological filter for reduction of noise instead of regular Gaussian regression or robust Gaussian regression approaches, median de-noising filter or spline noise procedure.

2. Materials and methods

Various type of surface texture were analysed, *e.g.* plateau-honed cylinder liners and cylinder textures containing additional burnished dimples, turned piston skirt details, grinded or isotropic textures. They were measured with a Talyscan 150 stylus instrument (nominal tip radius of about 2 μm, height resolution of about 10 nm, and measurement speed (velocity) between

Metrol. Meas. Syst., Vol. 27 (2020), No. 2, pp. 243–263
DOI: 10.24425/mms.2020.132772

0.1 mm s^{-1} (MV-1) and 0.5 mm s^{-1} (MV-5) or a Talysurf CCI Lite white light interferometer (height resolution 0.01 nm). The measured area was 5 mm by 5 mm (stylus method with 1000 × 1000 points) or 3.35 mm by 3.35 mm (non-stylus approaches with 1024 × 1024 points); the sampling interval and spacing were respectively 5 μm and 3.27 μm. More than 10 surfaces from each type were carefully considered but only a few of them were clearly presented in details. Examples of 3D or 2D results of stylus measurements at different velocity (also called "various conditions" in some cases) of texture containing oil-reservoir were presented in Fig. 1 and Fig. 2 respectively.

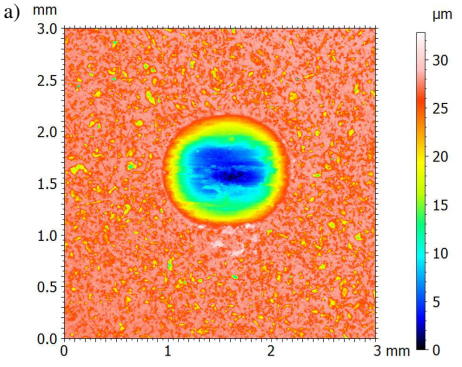

Sq = 5.05 μm,
Ssk = −2.57, *Sku* = 9.37,
Sp = 7.68 μm, *Sv* = 25.1 μm,
Sz = 32.8 μm,
Sa = 3.29 μm,
Sal = 0.511 mm,
Str = 0.798, *Std* = 0.276°,
Sdq = 0.354, *Sdr* = 5.9%,
Spd = 36.8 1/ mm^2, *Spc* = 0.195 1/ mm,
Sk = 3.69 μm, *Spk* = 1.81 μm, *Svk* = 4.1 μm

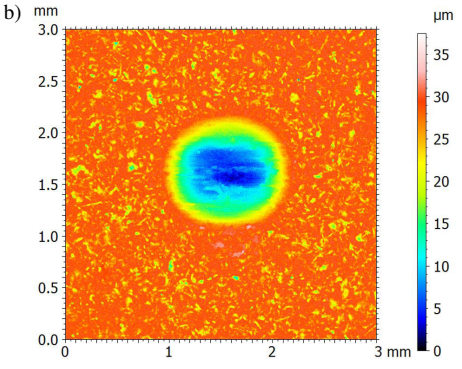

Sq = 5.12 μm,
Ssk = −2.46, *Sku* = 9.02,
Sp = 11 μm, *Sv* = 26.4 μm,
Sz = 37.4 μm,
Sa = 3.34 μm,
Sal = 0.51 mm,
Str = 0.8, *Std* = 0.268°,
Sdq = 0.626, *Sdr* = 18.4%,
Spd = 606 1/ mm^2, *Spc* = 0.448 1/ mm,
Sk = 4.33 μm, *Spk* = 1.71 μm, *Svk* = 3.9 μm

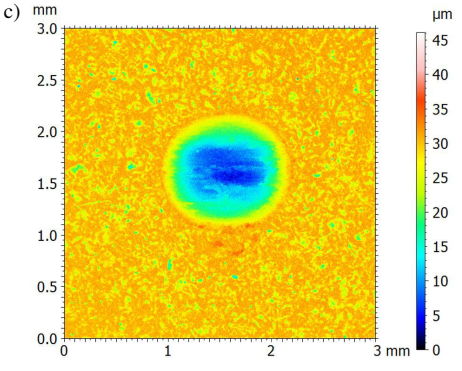

Sq = 5.26 μm,
Ssk = −2.27, *Sku* = 8.41,
Sp = 18 μm, *Sv* = 28.1 μm,
Sz = 46.1 μm,
Sa = 3.47 μm,
Sal = 0.506 mm,
Str = 0.8, *Std* = 0.267°,
Sdq = 0.961, *Sdr* = 42%,
Spd = 1512 1/ mm^2, *Spc* = 0.673 1/ mm,
Sk = 5.11 μm, *Spk* = 1.71 μm, *Svk* = 3.77 μm

Fig. 1. Contour plots and selected parameters of isotropic surface texture detail with center-distributed valley measured with various stylus conditions: MV-1 (a), MV-2 (b) and MV-3 (c).

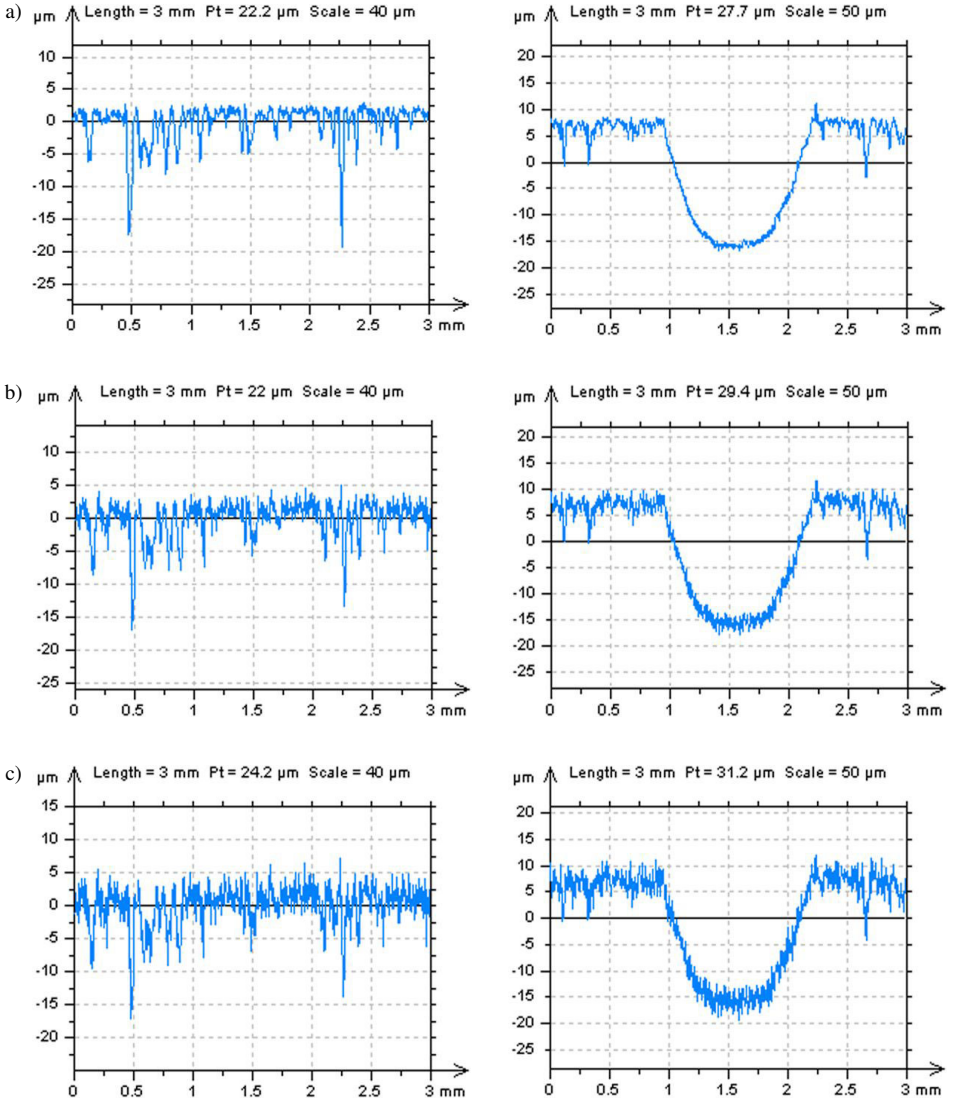

Fig. 2. Profiles with out-of-valley and/or center-valley locations (correspondingly) extracted from isotropic surface texture detail with center distributed valley presented in Fig. 1, measured with various stylus conditions: MV 1 (a), MV-2 (b) and MV-3 (c).

For extraction of some surface-features the following algorithms were applied and compared: *Gaussian Filter* (GF) or *Robust Gaussian Filter* (RGF), *Polynomial Fitted Plane of* 2^{nd} (PF2) or 4^{th} (PF4) degree, *Spline Filter* (SP), *Median De-Noising Filter* (MDNF), *Arithmetic Mean Filter* (AMF), *Fast Fourier Transform Filter* (FFTF), *High Envelope Filter* (HEF), *Low Envelope Filter* (LEF), *Closing-Opening* (COMF) or *Opening-Closing* (OCMF) *Morphological Filter*. Detection and reduction of noise were performed with defining *Noise Surface* (NS) as "removed results" of de-noising S-filtering approaches. Additionally, *Power Spectrum Density* (PSD) and *Autocorrelation Function* (AF) were studied for decreasing error size.

Metrol. Meas. Syst., Vol. 27 (2020), No. 2, pp. 243–263
DOI: 10.24425/mms.2020.132772

Selected parameters (from ISO 25178) were taken into account, as follows: arithmetic mean height *Sq*, skewness *Ssk*, kurtosis *Sku*, maximum peak height *Sp*, maximum valley depth (pit height) *Sv*, maximum height of surface *Sz*, arithmetic mean height *Sa*, auto-correlation length *Sal*, texture-aspect ratio (texture parameter) *Str*, texture direction *Std*, root mean square gradient (slope) *Sdq*, developed interfacial areal ratio *Sdr*, peak density *Spd*, arithmetic mean peak curvature *Spc*, core roughness depth (core height) *Sk*, reduced summit height *Spk*, reduced valley depth *Svk*. The influence of proposed feature-separation procedures (form extraction or noise reduction) on the values of parameters listed above was taken into account. The results obtained through application of proposed approaches (HEF or OCMF) were described in detail and compared with those after filtering with the generally-used procedures (GF, RGF, PF2, PF4, SP or MDNF).

3. Results and analysis

3.1. Envelope separation of surface features

Extraction of L-features was first taken into account with envelope characterisation compared with commonly-used algorithms. Envelope separation of surface features is defined as an envelope filtering of surface topography for decomposition and/or removal of unwanted components from the measurement results obtained. The bandwidth of all applied L-approaches was defined as equal to 0.8 mm according to the ISO standard [34] specification for areal separation of surface topography F-operator analysis. From the analysis of details contour plot (Fig. 3), where F-separated components were removed from measured data, it was assumed that the application of the regular GF caused the biggest distortion (flatness) of oil-reservoirs; similar results were obtained when RGF-extraction was applied for textures containing edge-located dimples (valley was classified as "edge-located" when its distance from the surface edge was smaller than half of its diameter).

It was also established in previous research that distortion of oil pockets has a tendency to increase enormously when the width of the valleys was greater than the filter cut-off value. In this case the application of a higher degree of RGF (2^{nd} [35] or greater) could not be justified. When the generally-used SF was adopted the oil pockets were still flattened. The view of the received results was disturbed by inflated/understated near-edge areas that are marked with the arrows in Fig. 3c, therefore, it was overlaid by the 3C-detail (out of near-edge distorted areas) extracted from the analysed element. Performing the above operation gave more precise "'eye-view"' information about some features' misstatement. The usage of SF caused a displacement both in the centre part of the valley and its adjacent areas in the textures considered. Contrary to the GF, RGF or SF "'eye-view"', dimple distortion (especially flattening) decreased when PF2, PF4 or HEF approaches were used. Nevertheless, for more direct confirmation of the schemes applied, assessment of surface topography parameters, specifically those characterizing the plateau-part and/or the valley-part of surface, should be carefully considered.

For the selection of an F-separation procedure for two-process (*e.g.* plateau-honed cylinder liner) surfaces, it was suggested to minimize the value of *Sk* and *Spk* parameters with simultaneously maximizing the *Svk* (due to this, valley flattening might be avoided). For analysed F-separating procedures the *Sk* parameter was minimized when GF was applied, nonetheless, *Svk* value was also the smallest; distortion, especially at the bottom part of the valleys was easy to observe. LEF can be applied to define the distortion of bottom-part of the oil-reservoirs (detail 3B in Fig. 3b results from this type of filtering method). When PF2 or PF4 procedures were applied, the value of *Svk* parameter increased, however, the *Sk* and *Spk* parameters also increased (follow-

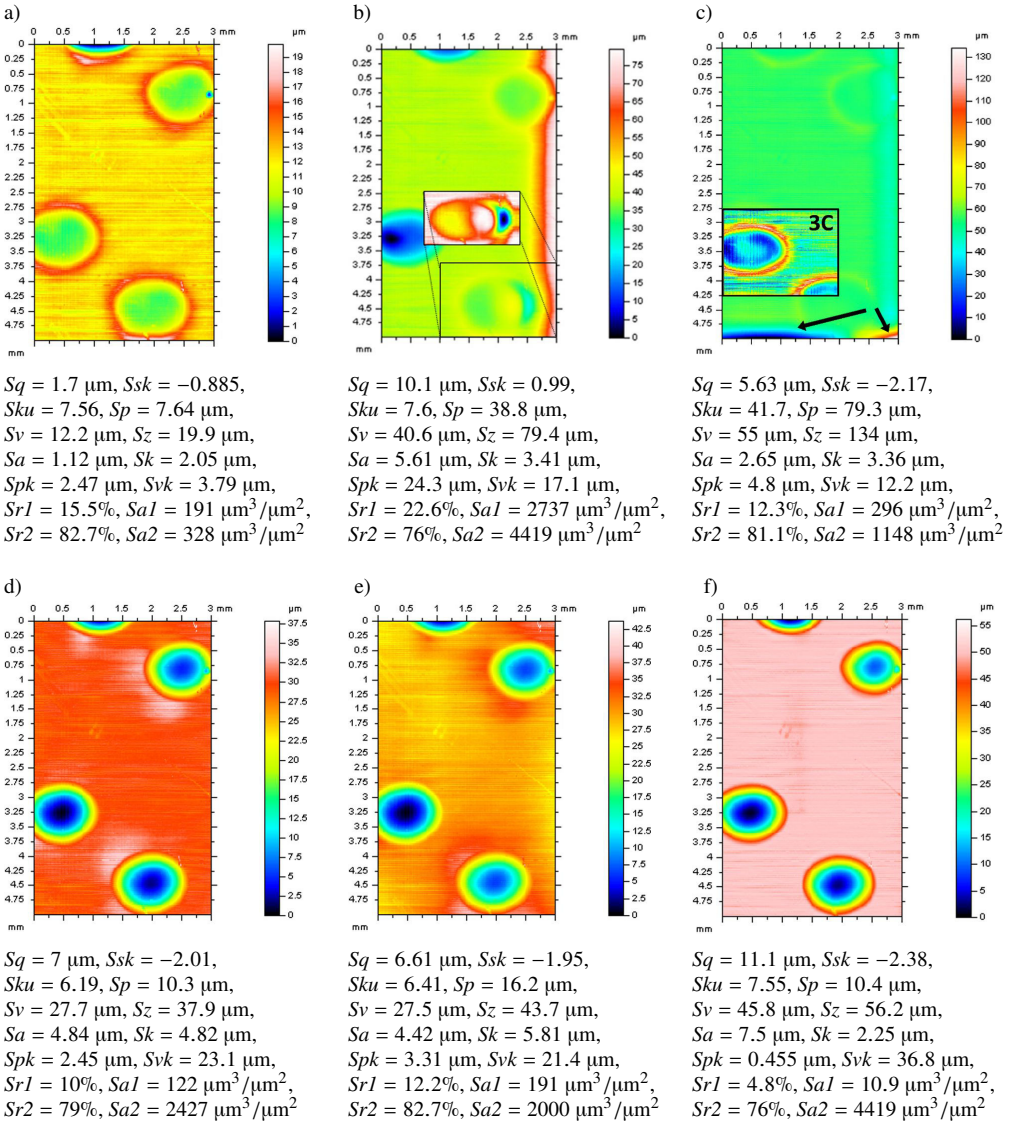

a) Sq = 1.7 µm, Ssk = −0.885, Sku = 7.56, Sp = 7.64 µm, Sv = 12.2 µm, Sz = 19.9 µm, Sa = 1.12 µm, Sk = 2.05 µm, Spk = 2.47 µm, Svk = 3.79 µm, $Sr1$ = 15.5%, $Sa1$ = 191 µm^3/µm^2, $Sr2$ = 82.7%, $Sa2$ = 328 µm^3/µm^2

b) Sq = 10.1 µm, Ssk = 0.99, Sku = 7.6, Sp = 38.8 µm, Sv = 40.6 µm, Sz = 79.4 µm, Sa = 5.61 µm, Sk = 3.41 µm, Spk = 24.3 µm, Svk = 17.1 µm, $Sr1$ = 22.6%, $Sa1$ = 2737 µm^3/µm^2, $Sr2$ = 76%, $Sa2$ = 4419 µm^3/µm^2

c) Sq = 5.63 µm, Ssk = −2.17, Sku = 41.7, Sp = 79.3 µm, Sv = 55 µm, Sz = 134 µm, Sa = 2.65 µm, Sk = 3.36 µm, Spk = 4.8 µm, Svk = 12.2 µm, $Sr1$ = 12.3%, $Sa1$ = 296 µm^3/µm^2, $Sr2$ = 81.1%, $Sa2$ = 1148 µm^3/µm^2

d) Sq = 7 µm, Ssk = −2.01, Sku = 6.19, Sp = 10.3 µm, Sv = 27.7 µm, Sz = 37.9 µm, Sa = 4.84 µm, Sk = 4.82 µm, Spk = 2.45 µm, Svk = 23.1 µm, $Sr1$ = 10%, $Sa1$ = 122 µm^3/µm^2, $Sr2$ = 79%, $Sa2$ = 2427 µm^3/µm^2

e) Sq = 6.61 µm, Ssk = −1.95, Sku = 6.41, Sp = 16.2 µm, Sv = 27.5 µm, Sz = 43.7 µm, Sa = 4.42 µm, Sk = 5.81 µm, Spk = 3.31 µm, Svk = 21.4 µm, $Sr1$ = 12.2%, $Sa1$ = 191 µm^3/µm^2, $Sr2$ = 82.7%, $Sa2$ = 2000 µm^3/µm^2

f) Sq = 11.1 µm, Ssk = −2.38, Sku = 7.55, Sp = 10.4 µm, Sv = 45.8 µm, Sz = 56.2 µm, Sa = 7.5 µm, Sk = 2.25 µm, Spk = 0.455 µm, Svk = 36.8 µm, $Sr1$ = 4.8%, $Sa1$ = 10.9 µm^3/µm^2, $Sr2$ = 76%, $Sa2$ = 4419 µm^3/µm^2

Fig. 3. Respective contour plots and topography parameters of cylinder liner surface contain oil reservoir valleys after feature-separation by: GF (a), RGF (b), SF (c), PF2 (d), PF4 (e) and proposed HEF (f).

ing the application of the GF, RGF or SF). The maximum (minimum) values of *Svk* (*Sk* and *Spk*) parameters were noticed when a HEF was proposed (from the applied algorithms). A very similar trend was observed for other height plateau-part or valley-part characterization parameters: *Sp* and *Sv* – decreasing and increasing respectively. Rest of the *Sk*-group/family parameters were minimized (*Sr1*, *Sa1*) or maximized (*Sr2*, *Sa2*) when surface F-texture was HEF-defined.

Some distortions and/or plateau-part of surface deformations were especially noticeable with profile assessments presented in Fig. 4. It was determined that the application of Gaussian algorithms for both regular regression filter and robust regression filtering caused a gross misin-

Metrol. Meas. Syst., Vol. 27 (2020), No. 2, pp. 243–263
DOI: 10.24425/mms.2020.132772

terpretation of features of oil-reservoir. Moreover, robust assessment creates a "bulge" especially in the edge-area of the detail considered where the height was bigger than the depth of the valley. The distortion was indicated by the arrow in Fig. 4b. Filtering with the widely used (commonly-available in commercial software) spline method caused an analogous (as against GR and RGF) exaggeration of valleys; nonetheless, the near-edge areas of dimples were less flattened. PF2 or PF4 extraction of L-components caused a smaller distortion of oil pockets although the error of form in the plateau-part of the profile was not entirely removed. The application of HEF caused the smallest misinterpretation of valley-features and plateau-parts of the profiles analysed.

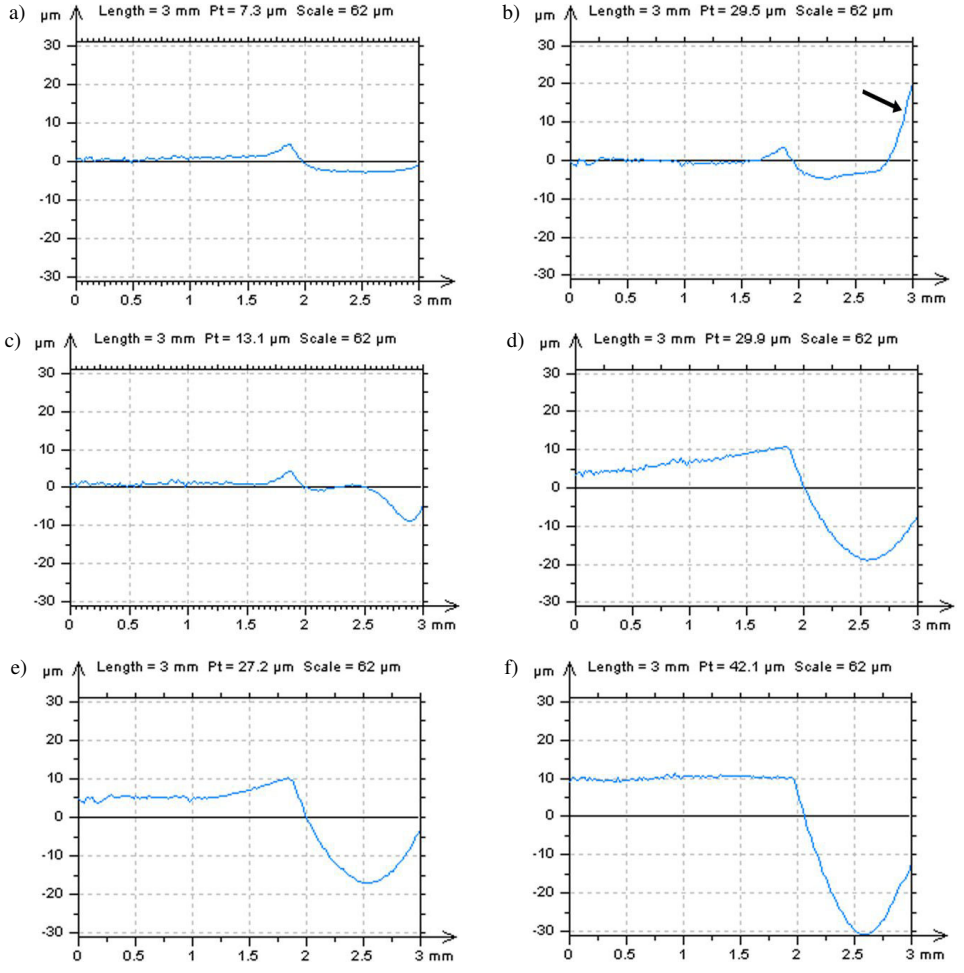

Fig. 4. Profiles from cylinder liner surface texture containing dimples after pre-processing with: GF (a), RGF (b), SF (c), PF2 (d), PF4 (e) and HEF (f).

3.2. Morphological reduction of measurement errors

The morphological reduction of measurement errors is defined as morphological filtration of surface texture applied to minimize some of the errors found in the measurement process. Reduction of measurement errors as S-results [34] was subsequently taken into consideration.

It was assumed that S-separated NS should contain only both high frequencies (or that these frequencies should be almost "entirely dominating" among all the NS frequencies; they were usually easy to find with a PSD analysis) and no features other than noise. When a PSD of RGF-defined NS (extracted from the plateau-honed cylinder liner surface) was taken into account, it was found that the extracted detail contains the high frequencies as the "dominant frequencies". Nonetheless, some features (scratches, dimple/valley-borders) were also removed from the measured values when "'eye-view"' assessments of NS were confirmed. Falsely decomposed features were not found in NSs defined by MDNF (*Multi-Dimensional Non-Linear Filtering* – another commercially-available procedure for surface topography noise reduction). However, the study of AF of an S-extracted NS showed that some features were still included in the noise; some non-high-frequency components can be found in the PSD diagram. The smallest value of the "dominating frequency" (defined by PSDs) of NS was obtained (0.05 mm) from regular de-noising procedures (RGF, MDNF and SF) when SF was applied; nonetheless, some treatment-features were still recognizable for both the NS contour map and the AF plot. No S-separated features on either NS or AF were observed when the HEF was applied. Moreover, the "peak-value" of the "'dominating-frequency"' was defined for 0.025 mm; it indicates that the HEF can be the best device (among the four presented and compared) for reduction of the high-frequency noise (with frequency approximately equal to 0.025mm) for two-process textures. The smaller number of non-noise features is removed from the measured data, the higher precision of surface texture parameter assessment can be received. The appliance of the HEF in noise reduction was similarly applied to topographies containing dimples. All the results are included in Fig. 5.

A similar thorough NS-evaluation was provided for turned or grinded details. The GF method caused a separation of non-noise components of data measured; in many cases the extracted elements had frequencies between 0.5 mm and 1.2 mm, but in more than 30% of studied grinded or turned details some components with frequencies equal to or bigger than 2 mm were noticed; exemplary GF- or MDNF-separated NS-details presented in Fig. 6 contained also frequencies equal to 1.5 mm, 1.7 mm, 2.4 mm and 3.35 mm of wavelength. Non-noise features (*e.g.* scratches and/or dimple sharp-edges) can be quickly noticed with AFs of NSs view. The number of NS non-noise features was the biggest (smallest) when GF (MDNF) was applied (from commercial regular approaches, *e.g.* GF, MDNF or SF). SF-defined NSs contain more small-scale frequencies (0.025 mm) than the other two procedures. This approach could be suggested for noise reduction albeit usually NSs and AFs contained traces of non-noise features. When OCMF-created NSs were observed neither non-noise features nor AFs-traces were found; the number of short-scale components (smaller than or equal to 0.025 mm) increased. The number of peak densities (values of *Spd* parameter) also increased significantly around 585%, 140% and 259% following the appliance of GF, MDNF and SF respectively; all the contour plot views, AFs and parameters calculation results of the analysed NS-details were presented in Fig. 6.

In Fig. 7 the most common errors in defining NSs were described and exposed. To reduce the noise from the results of turned texture measurement, the "eye-view" analysis was applied and assessments of MDNF-defined NSs assessments gave the most promising results. Nonetheless, the "dominating-frequency" in the NS was the 0.2 mm frequency for both, which also denies the usefulness of this type of filtration method, *i.e.* PSD and AF analyses. Some non-noise (any other than noise) features are barely noticeable in PSD examination when the GF was applied but in AFs or contour plot assessment they can be immediately observable. For plateau-honed cylinder liner textures with additionally burnished dimples the RGF application caused an extraction of some scratches, border/rim of valleys in the contour plot view of the NS, further assessment of PSDs or AFs is not required. For this type of texture the SF seems to be a better problem-solving and rational approach, especially when NS contour plots are considered. Nevertheless, when a

Metrol. Meas. Syst., Vol. 27 (2020), No. 2, pp. 243–263
DOI: 10.24425/mms.2020.132772

a)

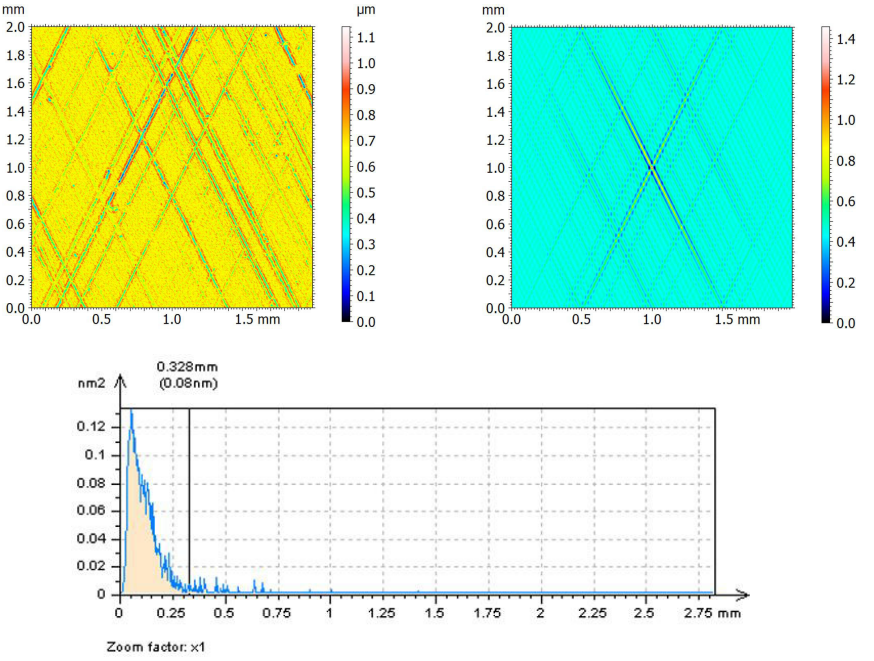

Sq = 0.0811 µm, *Ssk* = −0.949, *Sku* = 7.35, *Sp* = 0.466 µm, *Sv* = 0.676 µm, *Sz* = 1.14 µm, *Sa* = 0.0567 µm, *Smr* = 100%, *Smc* = 0.379 µm, *Sxp* = 0.202 µm, *Sal* = 0.00585 mm, *Str* = 0.0146, *Std* = 116°, *Sdq* = 0.0226, *Sdr* = 0.0256%, *Spd* = 1055 1/mm^2, *Spc* = 0.0148 1/mm

b)

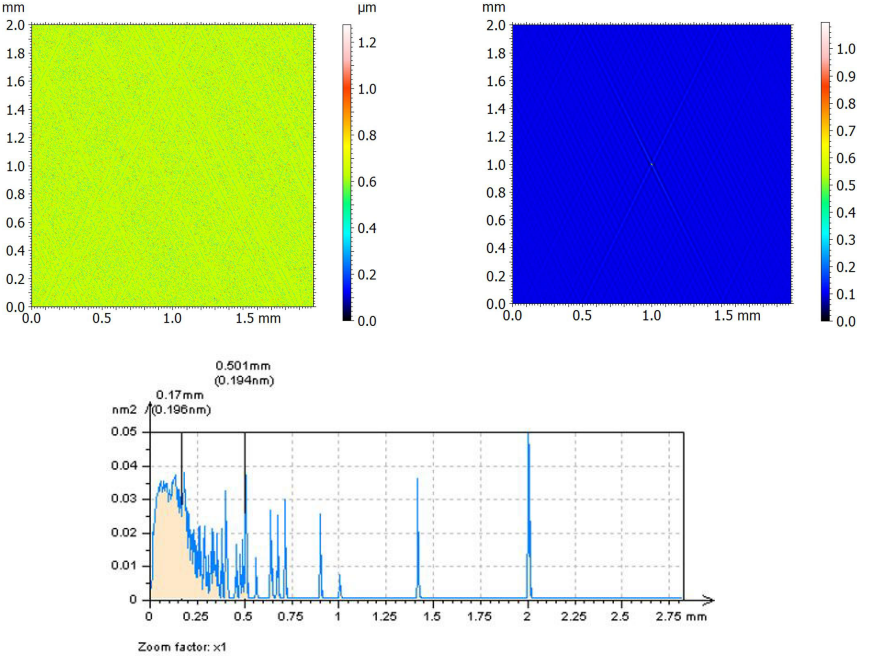

Sq = 0.0635 µm, *Ssk* = 0.628, *Sku* = 8.7, *Sp* = 0.632 µm, *Sv* = 0.644 µm, *Sz* = 1.28 µm, *Sa* = 0.0314 µm, *Smr* = 100%, *Smc* = 0.558 µm, *Sxp* = 0.138 µm, *Sal* = 0.00195 mm, *Str* = 0.353, *Std* = 116°, *Sdq* = 0.0415, *Sdr* = 0.0862%, *Spd* = 2627 1/mm^2, *Spc* = 0.0367 1/mm

c)

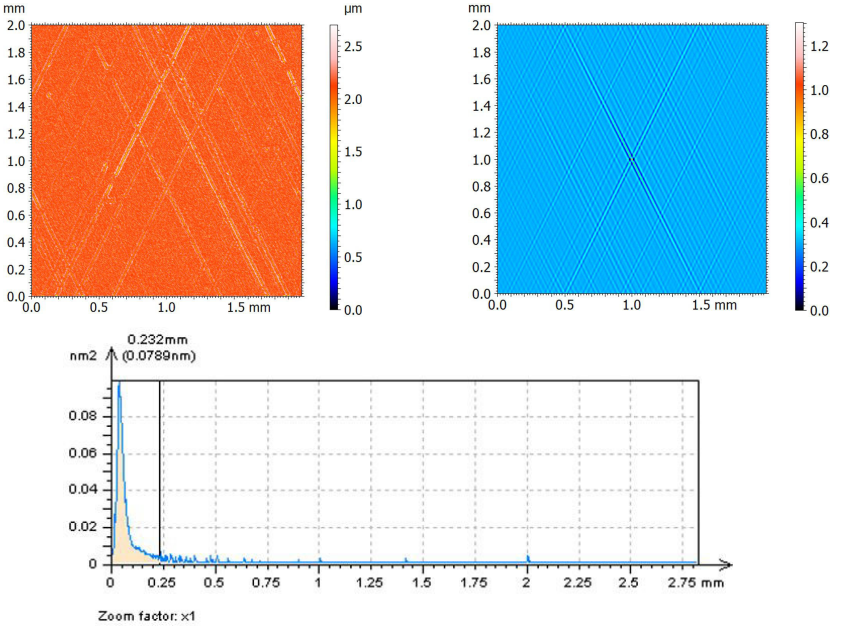

Sq = 0.109 µm, *Ssk* = −0.391, *Sku* = 7.08, *Sp* = 0.566 µm, *Sv* = 2.13 µm, *Sz* = 2.7 µm, *Sa* = 0.0839 µm, *Smr* = 99.9%, *Smc* = 0.432 µm, *Sxp* = 0.216 µm, *Sal* = 0.00276 mm, *Str* = 0.283, *Std* = 63.8°, *Sdq* = 0.0604, *Sdr* = 0.183%, *Spd* = 955 1/mm^2, *Spc* = 0.0451 1/mm

d)

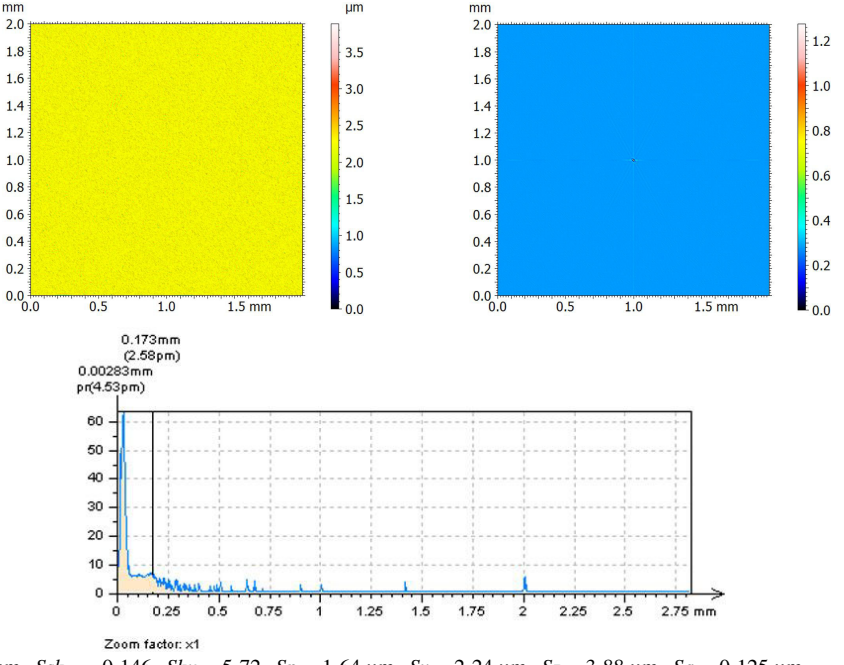

Sq = 0.159 µm, *Ssk* = −0.146, *Sku* = 5.72, *Sp* = 1.64 µm, *Sv* = 2.24 µm, *Sz* = 3.88 µm, *Sa* = 0.125 µm, *Smr* = 0.0388%, *Smc* = 1.44 µm, *Sxp* = 0.309 µm, *Sal* = 0*mm*, *Str* = 0, *Std* = 119°, *Sdq* = 0.108, *Sdr* = 0.578%, *Spd* = 1414 1/mm^2, *Spc* = 0.0831 1/mm

Fig. 5. Contour map plots, PSDs, AFs and parameters, respectively of NS decomposed from plateau-honed cylinder liner detail by application of: RGF (a), MDNF (b), SF (c) or HEF (d) approaches; cut-off = 0.025 mm.

Metrol. Meas. Syst., Vol. 27 (2020), No. 2, pp. 243–263
DOI: 10.24425/mms.2020.132772

a)

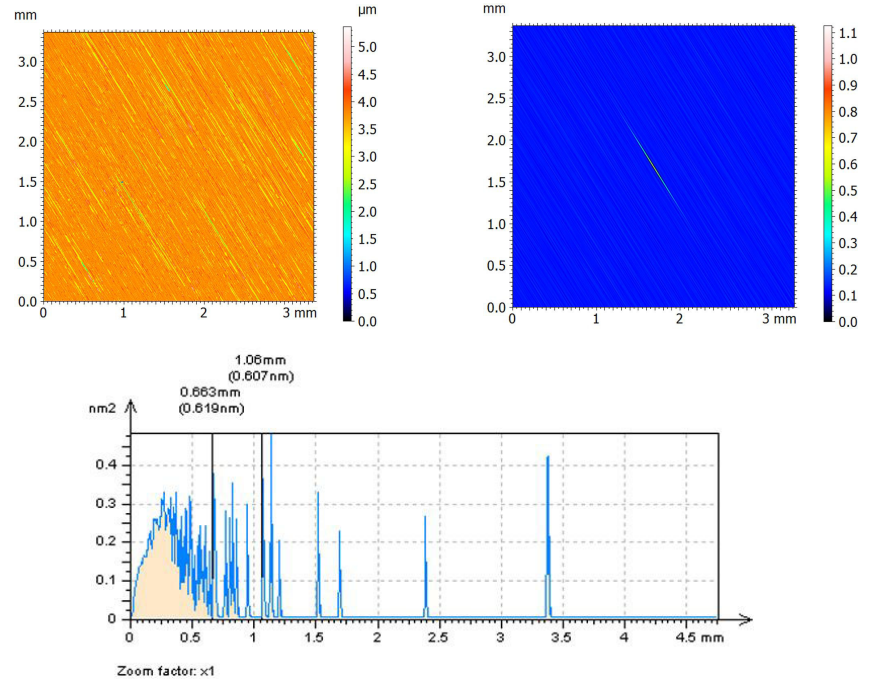

Sq = 0.21 µm, *Ssk* = −1.18, *Sku* = 9.68, *Sp* = 1.54 µm, *Sv* = 3.69 µm, *Sz* = 5.23 µm, *Sa* = 0.138 µm, *Smr* = 0.917%, *Smc* = 1.34 µm, *Sxp* = 0.559 µm, *Sal* = 0.00658 mm, *Str* = 0.0133, *Std* = 122°, *Sdq* = 0.0804, *Sdr* = 0.322%, *Spd* = 844 1/mm^2, *Spc* = 0.0723 1/mm

b)

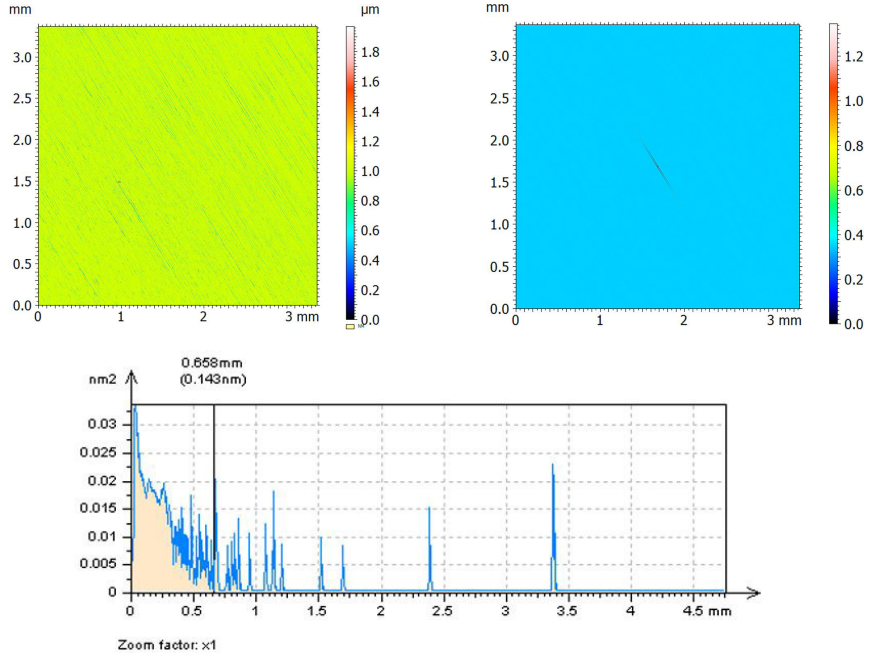

Sq = 0.0962 µm, *Ssk* = −0.139, *Sku* = 6.89, *Sp* = 0.955 µm, *Sv* = 1.01 µm, *Sz* = 1.97 µm, *Sa* = 0.0671 µm, *Smr* = 75.1%, *Smc* = 0.853 µm, *Sxp* = 0.21 µm, *Sal* = 0 mm, *Str* = 0, *Std* = 122°, *Sdq* = 0.0555, *Sdr* = 0.154%, *Spd* = 2408 1/mm^2, *Spc* = 0.0471 1/mm

c)

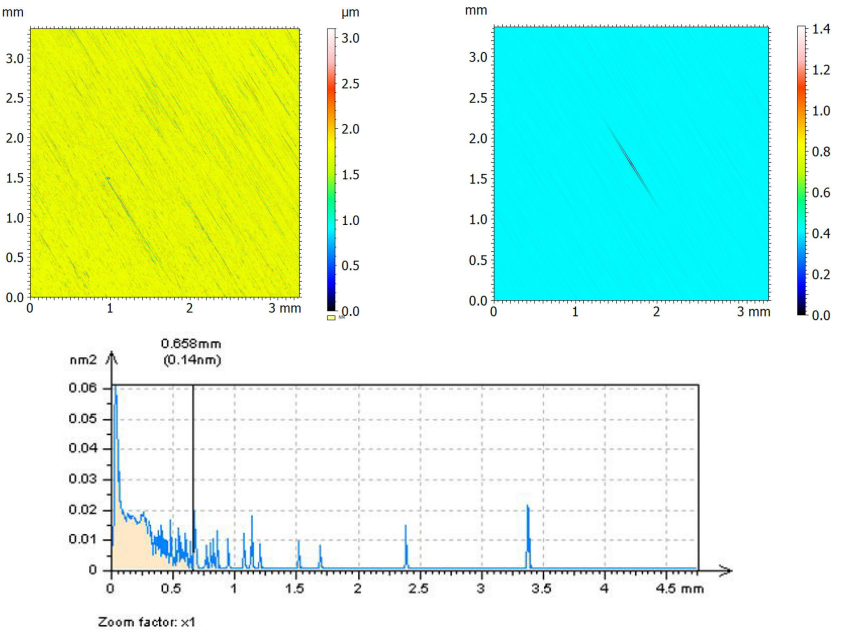

Sq = 0.155 µm, *Ssk* = −0.198, *Sku* = 5.18, *Sp* = 1.36 µm, Sv = 1.74 µm, *Sz* = 3.1 µm, *Sa* = 0.114 µm, *Smr* = 1.51%, *Smc* = 1.18 µm, *Sxp* = 0.339 µm, *Sal* = 0 mm, *Str* = 0, *Std* = 122°, *Sdq* = 0.0747, *Sdr* = 0.278%, *Spd* = 1610 1/mm^2, *Spc* = 0.0606 1/mm

d)

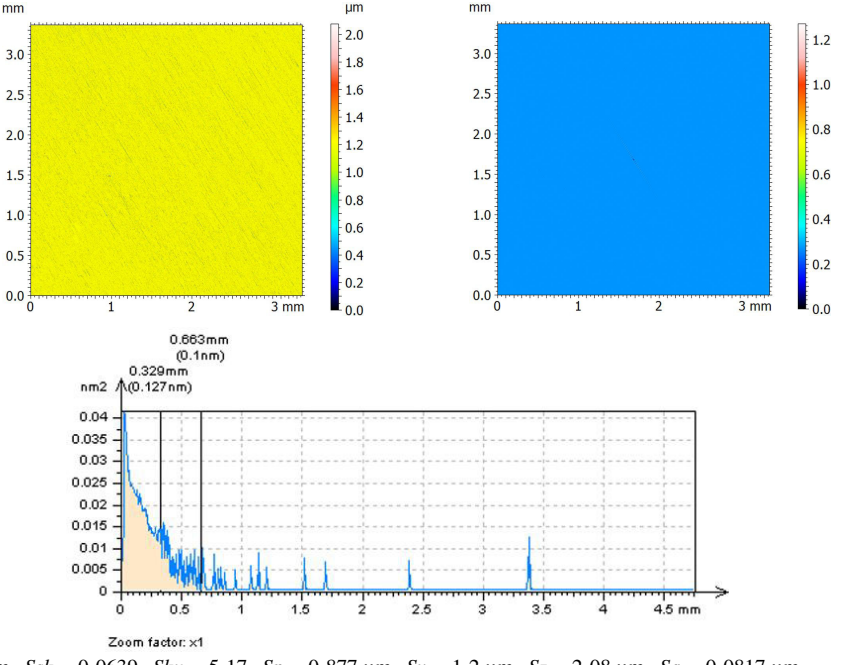

Sq = 0.11 µm, *Ssk* = 0.0639, *Sku* = 5.17, *Sp* = 0.877 µm, *Sv* = 1.2 µm, *Sz* = 2.08 µm, *Sa* = 0.0817 µm, *Smr* = 89.5%, *Smc* = 0.746 µm, *Sxp* = 0.22 µm, Sal = 0 mm, *Str* = 0, *Std* = 177°, *Sdq* = 0.0718, *Sdr* = 0.257%, *Spd* = 5781 1/mm^2, *Spc* = 0.0624 1/mm

Fig. 6. Contour map plots, PSDs, AFs and parameters, respectively, of NS from grinded detail decomposed with: GF (a), MDNF (b), SF (c) or OCMF (d) method; cut-off = 0.025 mm.

Metrol. Meas. Syst., Vol. 27 (2020), No. 2, pp. 243–263
DOI: 10.24425/mms.2020.132772

a) MDNF

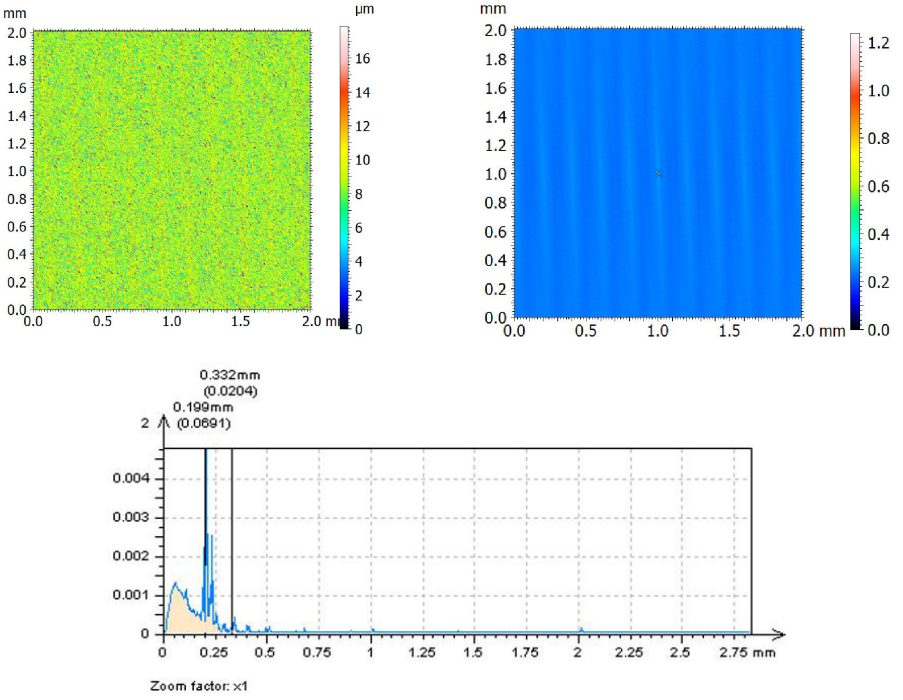

b) GF

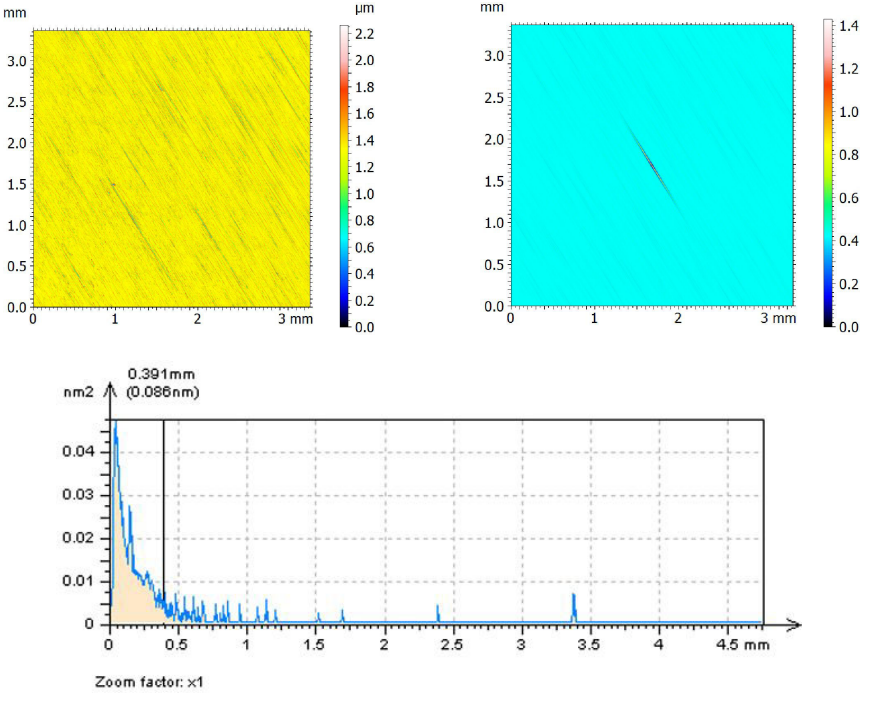

c) SF

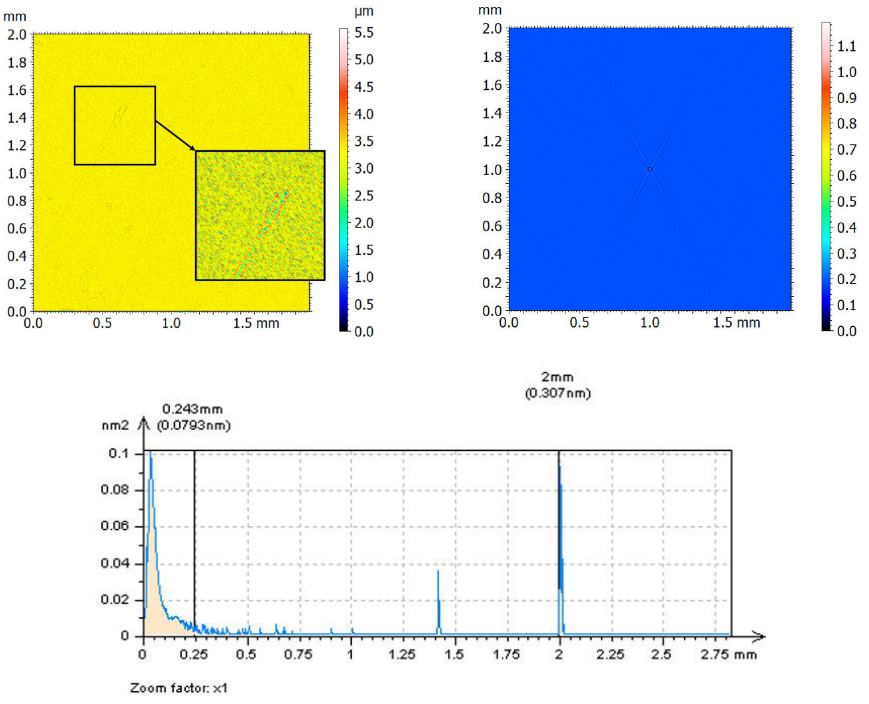
mm
μm
mm
0.243mm
(0.0793nm)
2mm
(0.307nm)
nm2
Zoom factor: x1

d) RGF

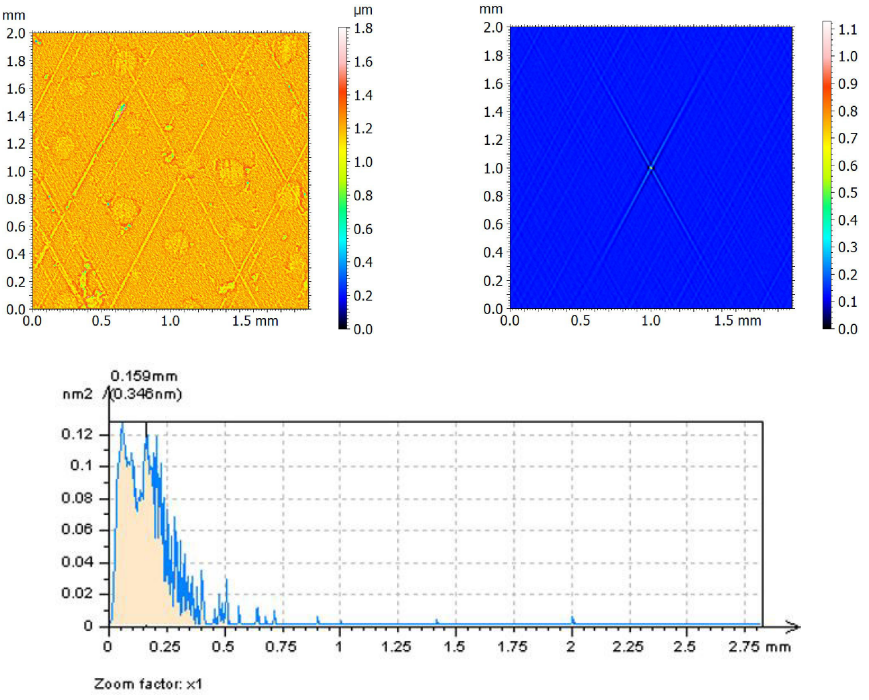
mm
μm
mm
0.159mm
(0.346nm)
nm2
Zoom factor: x1

Metrol. Meas. Syst., Vol. 27 (2020), No. 2, pp. 243–263
DOI: 10.24425/mms.2020.132772

e) COMF

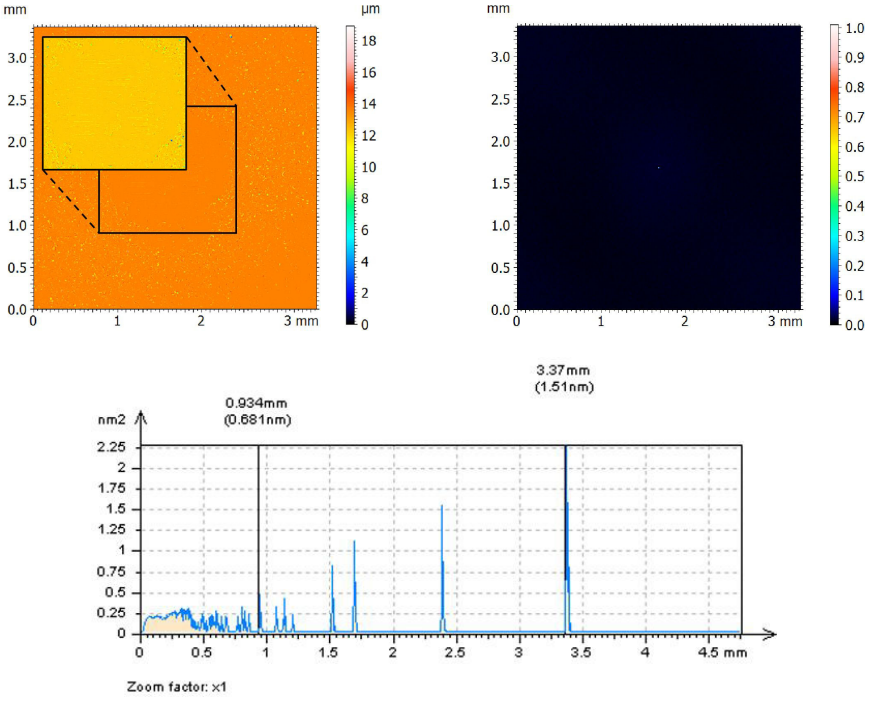

Fig. 7. Contour plots of NS, its PSD and AF, respectively, decomposed from: turned (a), grinded (b), plateau-honed (c) with additionally burnished dimples (d) and isotropic textures with deep/vide oil pockets (e), by application of various de-noising methods with cut-off equal to 0.025 mm.

part of the NS-detail was enlarged (Fig. 7c), the non-noise (unexpected in NSs) features were also found. Subsequently, the COMF-decomposition can be also used for non-practical applications where the surface contains deep/wide oil-reservoirs. Contour plots, PSDs or AFs analyses could not provide direct results; in some cases enlargement of dimple-areas in the NSs was required as follows in Fig. 7e. For describing the noise reduction procedure both "eye-view" of NSs with its parameters as well as PSDs or AFs assessments are required.

3.3. Proposal of envelope analysis of isotropic textures

Detection of non-noise features (*e.g.* scratches, dimples, borders/rims of valleys, sharp edges etc.) is utterly impossible in the analysis of isotropic surfaces – they do not exist in this type of textures. Therefore, the PSDs, AFs, parameter and profile analysis was reasonably required. An example of isotropic surface topography measured under various conditions was presented in Fig. 8. When noise was recognized (by profile analysis) in the measured data. it was assumed that *Sz*, *Sdr*, *Sk* and (which is obvious) *Spd*, *Spc* parameters increased the most; those parameters can be classified as "parameters susceptible on noise occurrence". Peak density increased more by than 7000%, it was always the parameter most sensitive to noise existence.

For detection and reduction of noise, various algorithms were tested: GF, RGF, MDNF, SP, AMF, OCMF, COMF and FFTF. For all of applied procedures "eye-view" assessment of the contour plot of NS did not allow to determine the occurrence of non-noise features; they were

a)

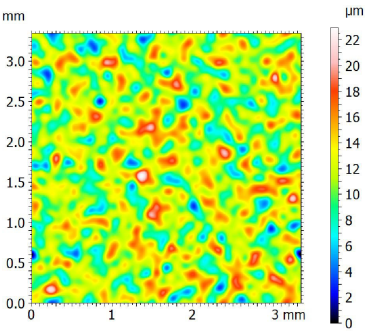

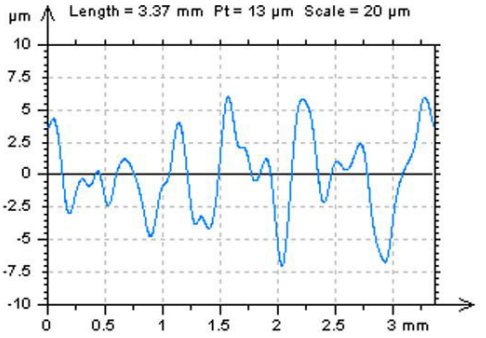

Sq = 2.84 μm, *Sp* = 11.3 μm, *Sv* = 11.6 μm, *Sz* = 22.9 μm, *Sa* = 2.25 μm, *Sal* = 0.212 mm, *Str* = 0.912, *Std* = 90°, *Sdq* = 0.0601, Sdr = 0.18%, *Spd* = 8.2 1/mm^2, *Spc* = 0.00188 1/mm, *Sk* = 6.31 μm, *Spk* = 2.48 μm, *Svk* = 2.44 μm

b)

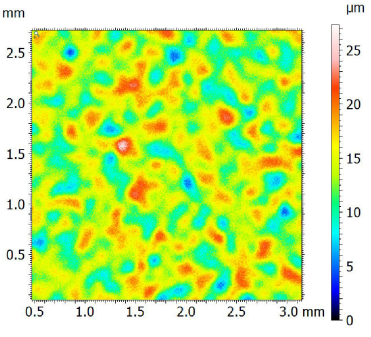

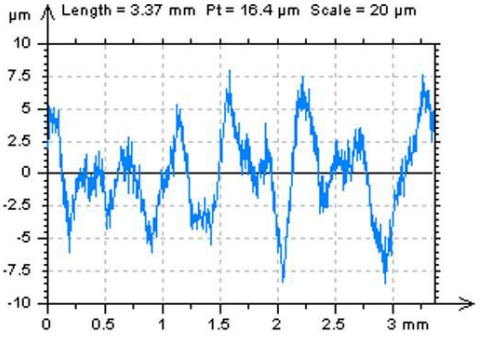

Sq = 2.97 μm, *Sp* = 13.7 μm, *Sv* = 13.7 μm, *Sz* = 27.3 μm, *Sa* = 2.36 μm, *Sal* = 0.207 mm, *Str* = 0.912, *Std* = 90°, *Sdq* = 0.362, *Sdr* = 6.38%, *Spd* = 612 1/mm^2, *Spc* = 0.216 1/mm, *Sk* = 6.65 μm, *Spk* = 2.5 μm, *Svk* = 2.57 μm

Fig. 8. Contour plots, example profiles and selected surface texture parameters of: MV-1 (a) and MV-5 (b) measured isotropic surface.

instantly visible with profile estimation. In Fig. 9 examples of NS-profiles decomposed by various pre-processing methods were presented. GF-NS contained an uneven distributed noise amplitude; it was established that the removed S-components consist of areas of noise concentration and areas were noise did not occur or its amplitude was negligible; the areas of noise-aggregation were indicated by the arrows in Fig. 9a. It was observed that application of OCMF or COMF caused errors in some NS-areas especially when two-separate beak-shaped surface summits were adjacent (usually the distance between them was smaller than 100 μm) and in the area between those tops a valley was situated whose width was greater than 25 μm (these types of errors were marked in profiles in Fig. 9b and 9c). Therefore, morphological operations (opening-closing and/or closing-opening) are not suggested for assessments of various isotropic textures, where the summit distribution was significantly varied the. Noise-separation with the MDNF caused a large scattering of NS *Sz* values; in some cases the difference was more of than 200% – it can be especially noticeable with an amplitude analysis of NS-profiles (Fig. 9d). The most logical and encouraging results were obtained when an FFTF was applied. Moreover, the NS-*Sz* value increases with the increase of the measurement speed; for 9 out of 10 NSs, the enlargement was proportional. the substantial maximum height differences were instantly recognized at the biggest measurement speed.

Metrol. Meas. Syst., Vol. 27 (2020), No. 2, pp. 243–263
DOI: 10.24425/mms.2020.132772

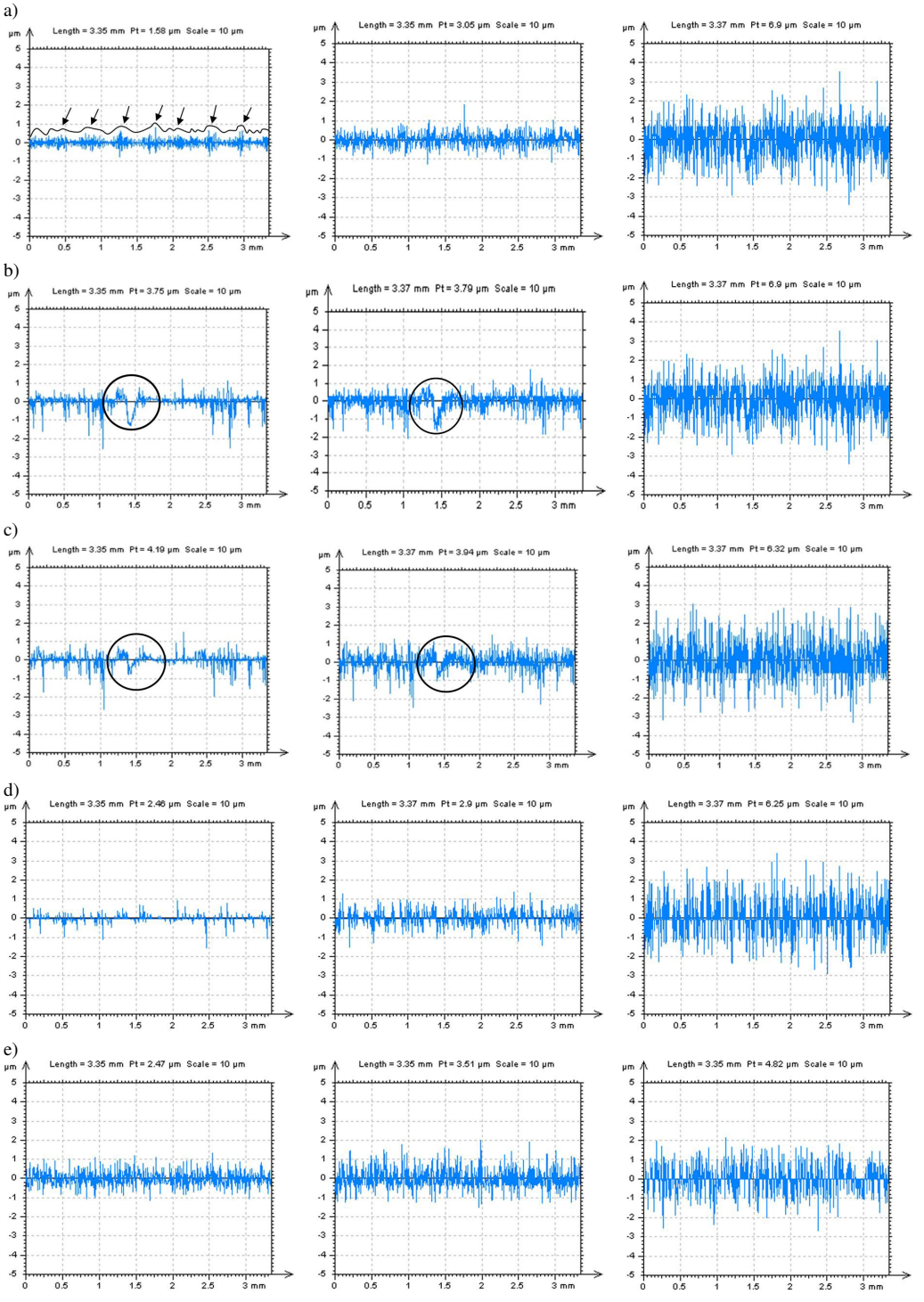

Fig. 9. Profiles extracted from NS defined with: GF (a), COMF (b), OCMF (c), MDNF (d), FFTF (e) procedure and, respectively, decomposed from MV 3, MV-4 and MV-5 measured isotropic surfaces.

A more detailed detection and subsequent assessment of noise or defining a NS in the PSD analysis can prove quite fundamental. In Fig. 10 the PSDs of NSs defined with various type of S-component extraction approaches were presented. It turned out that application of regular Gaussian filters (*e.g.* GF or RGF) caused an extraction of non-noise elements (with bandwidth equal to 0.25 mm). The usage of SF seemed to be effective enough (wavelengths from 0.25 mm to 1 mm did not occur). Nonetheless, components with mm frequency 2.35 were unnecessarily eliminated (from the data measured). For this reason, it was assumed that FFTF approaches reduce the expected frequencies in an optimal manner within the considered procedures. Small-scale components were the "dominating frequencies" or, more specifically, "entirely dominating frequencies". The non-noise frequency details in NSs were not particularly noticeable or did not exist.

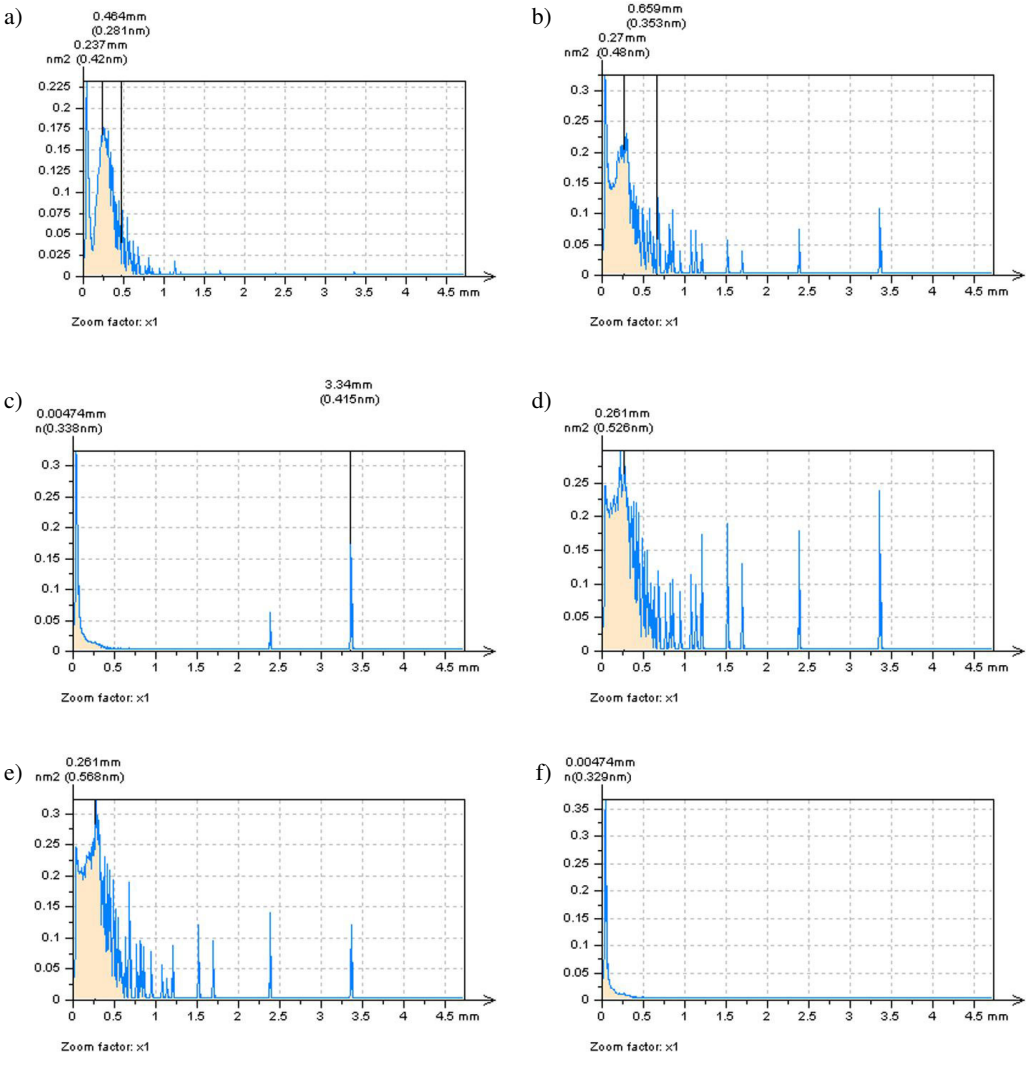

Fig. 10. PSDs of NSs decomposed from MV-5 measured isotropic surface by application of: GF (a), MDNF (b), SF (c), COMF (d), OCMF (e) or FFTF (f).

4. Conclusions

1. Extraction of F-components from surface topography measured data can be applied with the envelope filtering method. It is assumed that errors in areal form removal can be minimized when envelope characterization is used according to the commonly used and widely available procedures (*e.g.* regular Gaussian and robust Gaussian filtering methods, least-square fitted polynomials of 2^{nd} or 4^{th} degree, spline schemes). The direct and encouraging results are received especially when the plateau-honed cylinder liner texture with additionally burnished deep/wide dimples is taken into comprehensive and detailed account. In particular, the valley distribution, valley-to-valley and/or valley-to-edge distances should be also carefully considered.
2. Procedures for reduction of noise from the results of surface texture measurement process should be taken into consideration while applying the multi-threaded analysis. Selecting the noise reduction algorithm with characterization of noise surface as the result of removal of S-components from the data measured is suggested. It was also precisely defined that accurately extracted noise plane should contain only the S-components which can be directly verified with an in-depth power spectrum density analysis.
3. Power spectrum density, autocorrelation function and parameters of noise surface, especially those defined as noise-sensitive, should be simultaneously considered. If non-noise features are visible on the removed error-surface, then other methods should be directly applied. For plateau-honed cylinder liners, the Gaussian filters, usually offered in commercial software, caused an extraction of some non-noise marks, scratches, border/rim of valleys in the contour plot view of noise surface.
4. When turned or grinded details were taken into account, it was established that the application of the opening-closing morphological approach maximally reduced the number of non-noise features removed from the measured data. Moreover, the traces on the autocorrelation function diagram were also eliminated. when the contour plot view and/or autocorrelation function graph include some non-error features, the noise-reduction procedure should be subjected to amendment.
5. Selection of procedure for reduction of measurement noise in the analysis of isotropic surface topographies should be taken into careful consideration especially because this type of texture does not contain easily detected non-noise features (*e.g.* scratches, dimples, sharp edges); those features are not visible on the noise surface directly removed from the measured values.
6. For defining the noise surface (procedure for noise reduction/removal as well) the power spectrum density analysis seems to be justified. When the fast Fourier transform filter was applied, the small-scale components (surface/profile elements with high-frequencies) were found as "dominating frequencies" in the noise plane; the non-noise frequencies (as the noise was qualified within its high-frequency domain) were not detected and/or were absolutely negligible.
7. Minimization of pre-processing errors (*e.g.* extraction of F-, L- and/or S-components from surface texture measured data) and its influence on errors in surface topography parameters calculation/assessment should be approached with a multi-threaded sense. All "eye-view" and power spectrum density, autocorrelation function, parameter analysis should be obligatorily studied simultaneously.

Acknowledgements

This research was prepared with financial support from the National Science Centre, project No. 2013/09/N/ST8/04333.

References

[1] Hao, Q., Bianchi, D., Kaestner, M., Reithmeier, E. (2010). Feature based characterization of worn surfaces for a sliding test. *Tribology International*, 43(5–6), 1186–1192.

[2] Li, L., Zhang, X., Zhang, H., He, X., Xu, M. (2010). Feature extraction of non-stochastic surfaces using curvelets. *Precision Engineering*, 39, 212–219.

[3] Vorburger, T.V., Rhee, H.-G., Renegar, T.B., Song, J.-F., Zheng, A. (2007). Comparison of optical and stylus methods for measurement of surface texture. *The International Journal of Advanced Manufacturing Technology*, 33(1–2), 110–118.

[4] Pawlus, P., Reizer, R., Wieczorowski, M. (2018). Comparison of results of surface texture measurement obtained with stylus methods and optical methods. *Metrology and Measurement Systems*, 25(3), 589–602.

[5] Srivastava, D., Agarwal, A. (2004). Experimental investigations on the effect of liner surface properties on wear in non-firing engine simulator. *SAE Technical Paper*, 1, 0605.

[6] Podulka, P, Dobrzański, P, Pawlus, P, Lenart, A. (2014). The effect of reference plane on values of areal surface topography parameters from cylindrical elements. *Metrology and Measurement Systems*, 21(2), 247–256.

[7] De Groot, P.J. (2019). A review of selected topics in interferometric optical metrology. *Reports on Progress in Physics*, 82(5), 056101.

[8] De Groot, P.J. (2015). Principles of interference microscopy for the measurement of surface topography. *Advances in Optics and Photonics*, 7(1), 1–65.

[9] Poon, C.Y., Bhushan, B. (1995). Comparison of surface roughness measurements by stylus profiler, AFM and non-contact optical profiler. *Wear*, 190(1),76–88.

[10] Podulka, P., Pawlus, P., Dobrzański, P., Lenart, A. (2014). Spikes removal in Surface measurement. *Journal of Physics: Conference Series*, 483, 012025.

[11] Jiang, X., Lou, S., Scott, P.J. (2012). Morphological method for surface metrology and dimensional metrology based on the alpha shape. *Measurement Science and Technology*, 23(1), 015003.

[12] Pawlus, P., Reizer, R., Wieczorowski, M. (2017). Problem of non-measured points in surface texture measurements. *Metrology and Measurement Systems*, 24(3), 525–536.

[13] Whitehouse, D. (2011). Surface metrology today: complicated, confusing, effective. *Proc. of the 13th International Conference on Metrology and Properties of Engineering Surfaces*, Twickenham Stadium, United Kingdom, 1–10.

[14] De Groot, P.J. (2017). The meaning and measure of vertical resolution in optical surface topography measurement. *Applied Sciences*, 7(1), 54.

[15] Abdelsalam, D.G., Kim, D. (2011). Coherent noise suppression in digital holography based on flat fielding with apodized apertures. *Optics Express*, 19(19), 17951.

[16] Xu, X., Huang, Q., Shen, Z., Wang, Z. (2016). Improving the surface metrology accuracy of optical profilers by using multiple measurements. *Optical Engineering*, 55(10), 104105.

Metrol. Meas. Syst., Vol. 27 (2020), No. 2, pp. 243–263
DOI: 10.24425/mms.2020.132772

[17] Giusca, C.L., Leach, R.K., Helary, F., Gutauskas, T., Nimishakavi, L. (2012). Calibration of the scales of areal surface topography-measuring instruments: part 1. Measurement noise and residual flatness. *Measurement Science and Technology*, 23(3), 035008.

[18] Jiang, X., Scott, P.J., Whitehouse, D.J., Blunt, L. (2007). Paradigm shifts in surface metrology. Part II. The current shift. *Proceedings of The Royal Society A*, 463(2085), 2071–2099.

[19] Rahlves, M., Roth, B., Reithmeier, E. (2017). Confocal signal evaluation algorithms for surface metrology: uncertainty and numerical efficiency. *Applied Optics*, 56(21), 5920–5926.

[20] Lou, S., Jiang, X., Scott, P.J. (2013). Application of the morphological alpha shape method to the extraction of topographical features from engineering surfaces. *Measurement*, 46(2), 1002–1008.

[21] Lou, S., Jiang, X., Scott, P.J. (2014). Fast algorithm for Morphological Filters. *Journal of Physics: Conference Series*, 311, 012001.

[22] Lou, S., Jiang, X., Scott, P.J. (2013). Correlating motif analysis and morphological filters for surface texture analysis. *Measurement*, 46(2), 993–1001.

[23] Kumar, J., Shunmugam, M.S. (2006). Morphological operations on engineering surfaces using a 3D-structuring element of an appropriate size. *Measurement Science and Technology*, 17(10), 2655.

[24] Pawlus, P., Reizer, R., Łętocha, A., Wieczorowski, M. (2019). Morphological filtration of two-process profiles. *Bulletin of the Polish Academy of Science Technical Science*, 67(1), 107–113.

[25] Kumar, J., Shunmugam, M.S. (2006). A new approach for filtering of surface profiles using morphological operations. *International Journal of Machine Tools and Manufacture*, 46(3–4), 260–270.

[26] Lou, S., Jiang, X., Scott, P.J. (2012). Algorithms for morphological profile filters and their comparison. *Precision Engineering*, 36(3), 414–423.

[27] Tholath, J., Radhakrishnan, V. (1999). Three-dimensional filtering of engineering surfaces using envelope system. *Precision Engineering*, 23(4), 221–228.

[28] Dietzsch, M., Gerlach, M., Groeger, S. (2008). Back to the envelope system with morphological operations for the evaluation of surfaces. *Wear*, 264(5–6), 411–415.

[29] Lingadurai, K., Shunmugam, M.S. (2005). Use of morphological closing filters for three-dimensional filtering of engineering surfaces. *Journal of Manufacturing Systems*, 24(4), 366–376.

[30] Janecki, D. (2011). Gaussian filters with profile extrapolation. *Precision Engineering*, 35(4), 602–606.

[31] Kumar, J., Shunmugam, M.S. (2007). Fitting of robust reference surface based on least absolute deviations. *Precision Engineering*, 31(2), 102–113.

[32] Jiang, X. (2010). Robust solution for the evaluation of stratified functional surfaces. *CIRP Annals – Manufacturing Technology*, 59(1), 573–576.

[33] Zhang, H., Yuan, Y., Piao, W. (2010). A universal spline filter for surface metrology. *Measurement*, 43(10), 1575–1582.

[34] ISO 25178-3:2012 Geometrical product specifications (GPS) – Surface texture: Areal – Part 3: Specification operators.

[35] Brinkmann, S., Bodschwinna, H. (2003). Advanced Gaussian filters. Blunt L., Jiang X. (eds.). *Advanced Techniques for Assessment Surface Topography*. London and Sterling: Kogan Page Science, 62–89.